remote sensing

MDPI

Article

Slow-Time MIMO Waveform Design Using Pulse-Agile-Phase-Coding for Range Ambiguity Mitigation

Shaoqiang Chang [1,2], Fawei Yang [1], Zhennan Liang [1,*], Wei Ren [3], Hao Zhang [1] and Quanhua Liu [1,3]

[1] Radar Research Lab, School of Information and Electronics, Beijing Institute of Technology, Beijing 100081, China; shaoqiangchang@bit.edu.cn (S.C.); yangfawei@bit.edu.cn (F.Y.); 3120220767@bit.edu.cn (H.Z.); liuquanhua@bit.edu.cn (Q.L.)
[2] Beijing Institute of Technology Chongqing Innovation Center, Chongqing 401120, China
[3] Department of Computing, The Hong Kong Polytechnic University, Hong Kong 999077, China; wei-2022.ren@polyu.edu.hk
* Correspondence: liangzhennan@bit.edu.cn

Abstract: This paper proposed a Pulse-Agile-Phase-Coding slow-time MIMO (PAPC-st-MIMO) waveform, where the phase-coded signal is utilized as the intra-pulse modulation of the slow-time MIMO waveform. Firstly, the signal model of the proposed waveform is derived. To improve the orthogonality of the phase-coded waveform sets, a novel hybrid evolutionary algorithm based on Cyclic Algorithm New (CAN) is proposed. After the optimization process of the phase-coded waveform sets, the signal processing method of the PAPC-st-MIMO waveform is derived. Finally, the effectiveness of the proposed method is verified with a simulation experiment. The mitigation ratio of the near-range detection waveform can achieve −30 dB, while the long-range detection waveform can achieve −35 dB. This approach ensures waveform orthogonality while enabling the slow-time MIMO waveform to achieve distance selectivity. By conducting joint pulse-Doppler processing across multiple range segments, range ambiguity can be suppressed, increasing the system's Pulse Repetition Frequency (PRF) without introducing ambiguity.

Keywords: slow-time MIMO radar; pulse agile phase-coding; MIMO radar waveform design; MIMO radar range ambiguity mitigation

Citation: Chang, S.; Yang, F.; Liang, Z.; Ren, W.; Zhang, H.; Liu, Q. Slow-Time MIMO Waveform Design Using Pulse-Agile-Phase-Coding for Range Ambiguity Mitigation. *Remote Sens.* **2023**, *15*, 3395. https://doi.org/10.3390/rs15133395

Academic Editor: Andrzej Stateczny

Received: 15 June 2023
Revised: 29 June 2023
Accepted: 2 July 2023
Published: 4 July 2023

1. Introduction

As a novel radar system, multiple-Input Multiple-Output (MIMO) radar transmits orthogonal waveforms and separates the echoes corresponding to each transmitting channel at the receiving end. This capability allows MIMO radar to achieve virtual aperture extension. The waveform diversity characteristic of MIMO radar enables it to exhibit exceptional performance in several aspects, including low-speed target detection [1,2], angle estimation [3,4], and clutter suppression [5,6], unlike those conventional MIMO techniques which conduct in the fast-time such as Frequency Division Multiple Access (FDMA) and Code Division Multiple Access (CDMA), slow-time MIMO typically requires joint processing of multiple pulses within a CPI to achieve orthogonal transmitting. The slow-time MIMO waveforms mainly include Time Division Multiple Access (TDMA) and DDMA [7–11].

The Doppler Division Multiple Access (DDMA) waveforms introduce an initial linear phase to each transmitting channel within a Coherent Processing Interval (CPI), thereby achieving orthogonality in the Doppler domain. Additionally, the DDMA waveform demonstrates high clutter correlation and excellent clutter suppression performance, as each channel's transmitted signal shares the same carrier frequency [12–15]. DDMA has found widespread applications in various fields, including autonomous driving [16] and urban security [17,18].

In 2018, Texas Instruments (TI) introduced the AWR1843, a 77 GHz Frequency-Modulated Continuous Wave (FMCW) MIMO automotive mmWave radar module. This module incorporates three transmit channels and four receive channels, enabling the transmission of slow-time MIMO waveforms [19]. Reference [20] conducted target detection experiments using this radar module and compared its performance with Single-Input Multiple-Output (SIMO) radar. The study analyzed the enhancement in target angle resolution achieved by the slow-time FMCW MIMO radar.

Furthermore, reference [21] developed a low, slow, and small (LSS) target detection radar system based on the Doppler Division Multiple Access (DDMA) waveform. They proposed a clutter suppression method for slow-time MIMO radar, utilizing independent component analysis. The research team tested the radar system's effectiveness in detecting small unmanned aerial vehicle (UAV) targets [22].

In the Doppler domain, slow-time MIMO radar introduces waveform diversity, significantly reducing the Doppler unambiguous region for each receive-transmit channel pair. To address issues related to target velocity ambiguity and blind velocity suppression in slow-time MIMO radar, researchers have conducted a series of studies. In 2011, reference [23] proposed two methods, Frequency-Dithered DDMA and Phase-Dithered DDMA, to tackle the blind velocity problem associated with DDMA waveforms. Frequency-Dithered DDMA modifies the mapping relationship between the Doppler sub-bands of the transmitted signal and the transmitting elements in a nonlinear manner, effectively suppressing blind velocities of non-array normal targets. On the other hand, Phase-Dithered DDMA introduces random phase perturbations to each channel and achieves the suppression of blind velocities, including those of array normal targets, through matched reception. In 2012, reference [24] further enhanced the theoretical framework of dithered DDMA and analyzed the performance of the DDMA waveform in terms of clutter cancellation ratio (CR). The computational complexity of dithered DDMA is low. However, when using matched filtering for signal processing, there will be high sidelobes and target SINR loss, affecting weak targets' detection effect.

In 2018, reference [25] introduced the Random Slow-Time Code Division Multiple Access (ST-CDMA) waveforms. This waveform employs random initial phases for each pulse and incorporates Sparse Signal Processing (SSP) techniques to mitigate the target velocity ambiguity encountered in conventional DDMA waveforms. Furthermore, it effectively suppresses the high sidelobes induced by matched filtering. However, it is essential to note that SSP involves nonlinear processing, resulting in elevated computational complexity.

Reference [26] conducted a study on methods for blind velocity suppression in DDMA using multiple frequencies and multiple Pulse Repetition Frequencies (PRFs). The multiple-frequency blind velocity suppression method imposes requirements on the system bandwidth. It increases hardware complexity, while based on the Chinese Remainder Theorem, the multiple-PRF method is highly sensitive to errors. Reference [27] employed the parallel factorization method to jointly estimate target parameters in slow-time MIMO radar to address the target velocity ambiguity issue. However, tensor decomposition-based methods exhibit high computational complexity, unstable algorithm convergence, and require auxiliary conditions to ensure convergence to the optimal solution.

The current methods for blind velocity suppression and target velocity ambiguity resolution in slow-time MIMO radar have advantages and limitations, including high sidelobe, sensitivity to errors and high computational complexity in nonlinear processing. This study employs a straightforward approach to address the limitation of increasing the system's Pulse Repetition Frequency to expand the unambiguous velocity range of DDMA waveforms. However, raising the PRF leads to a significant target range ambiguity problem. The paper proposes a range ambiguity suppression method for slow-time MIMO radar based on intra-pulse waveform agile phase coding to overcome this issue.

The proposed method introduces the Pulse-Agile-Phase-Coding slow-time MIMO (PAPC-st-MIMO) waveform, where the phase-coded signal is utilized as the intra-pulse modulation of the slow-time MIMO waveform. This approach ensures waveform orthogo-

nality while enabling the slow-time MIMO waveform to achieve distance selectivity. By conducting joint pulse-Doppler processing across multiple range segments, range ambiguity can be suppressed, increasing the system's PRF without introducing ambiguity.

2. Methodology

2.1. Signal Model

Consider a co-located 1D linear antenna array with M transmitting elements that are omnidirectional. The element distance to the reference antenna of the mth, $m = 0, \ldots, M-1$ element in the transmitting array is d_m. Note that this definition of the array is general regardless of whether the array is uniform or not. The operating frequency is f_0 and the operating wavelength is λ_0. There are K pulses in one CPI and the PRF $f_r = 1/T_r$, where T_r refers to pulse repetition interval (PRI).

The slow-time MIMO approach split the whole Doppler PRF into M orthogonal Doppler sub-bands with a bandwidth of $\Delta f_{sub} = f_r/M$ via slow-time phase coding. Here, we set the number of the Doppler sub-bands as the same as the number of transmitting antennas to simplify the modeling. Furthermore, the Doppler sub-bands can be redundant, leading to some empty Doppler sub-bands that can be utilized to enlarge the velocity measurement range. The baseband pulse waveform $u_{pulse}(t)$ has varying starting phases $\varphi(m,k)$, a function of the transmitting element index m and the pulse index (slow-time) k. The transmitting waveform of the mth element is:

$$s_m(t) = \sum_{k=0}^{K-1} u_{pulse}(t - kT_r) e^{j2\pi(f_0 t + \varphi(m,k))} \tag{1}$$

The PAPC-st-MIMO waveform uses phase-coded signals as the pulse modulation method. It is assumed that there are Q different continuous phase-coded signals in a frame of a PAPC-coded signal set $\left\{u^q_{pulse}(t)\right\}, (q = 0, \ldots, Q-1)$, and the code length of each coded signal is P bits. Then the pulse modulation waveform of the group phase-coded signal can be expressed as:

$$u^q_{pulse}(t) = \frac{1}{\sqrt{P}} \sum_{p=0}^{P-1} c_{qp} rect\left(\frac{t - p\tau_c - \frac{\tau_c}{2}}{\tau_c}\right), \tag{2}$$

where $\left\{c_{qp}\right\}, (p = 0, \ldots, P-1)$ is the coding sequence of the q-th group phase-coded signal, τ_c the chip width, and the interval between two adjacent chips. Therefore, the baseband reference signal model of a frame of PAPC coded signal set can be obtained by:

$$u_{ref}(t) = \frac{1}{\sqrt{PQ}} \sum_{q=0}^{Q-1} \sum_{p=0}^{P-1} c_{qp} rect\left(\frac{t - p\tau_c - \frac{\tau_c}{2} - qT_r}{\tau_c}\right). \tag{3}$$

The PAPC pulse modulation waveform represented by (3) is brought into (1), and the PAPC-st-MIMO transmission signal model corresponding to the mth transmit antenna can be obtained:

$$s\prime_m(t) = \sum_{r=0}^{K/Q-1} \sum_{q=0}^{Q-1} u^q_{pulse}\left(t - qT_r - rT_Q\right) e^{j2\pi(f_0 t + \varphi(m, r\times Q+q))}, \tag{4}$$

where $T_Q = QT_r$ is the frame period of the PAPC signal, the ratio of the number of pulses in the CPI to the number of PAPC signals in a frame, $R = K/Q$, is selected as an integer to simplify the model. The transmission waveform of the PAPC-st-MIMO signal is shown in Figure 1. The PAPC-coded signal set can obtain a signal set with good auto/cross-correlation characteristics through the optimization search algorithm, and its design process will be described in detail in the next section.

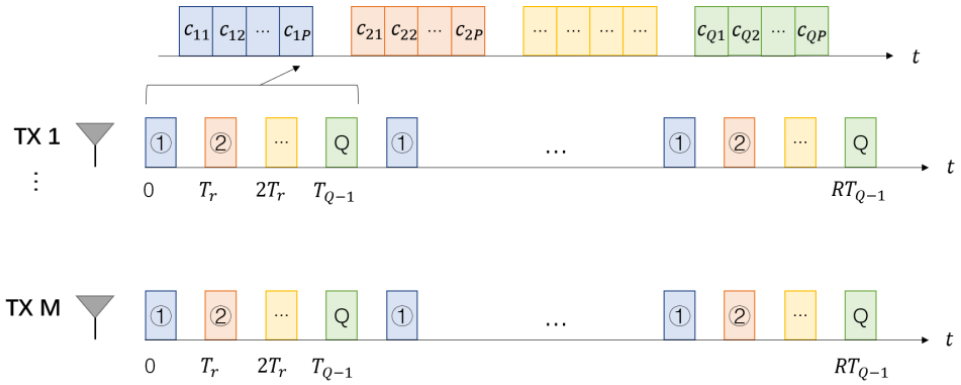

Figure 1. Schematic diagram of PAPC-st-MIMO waveform.

2.2. PAPC Signal Set Design

This section provides a detailed introduction to the design method of orthogonal phase-coded signal sets. Firstly, the principles of the Evolutionary Algorithm (EA) and Cyclic Algorithm New (CAN) are introduced, respectively. Then, the hybrid algorithm based on evolutionary algorithm and a new cyclic algorithm: the EA-CAN algorithm, is introduced, and the advantages of this algorithm compared with traditional algorithms are analyzed.

An evolutionary algorithm is a class of stochastic optimization algorithms under the new Darwinian paradigm, where the new Darwinian paradigm is a combination of classical Darwinian evolution, Weismann's selection theory, and Mendelian genetics [28]. Classic genetic algorithms (GA), memetic algorithms (MA), etc., belong to evolutionary algorithms. The main operations of evolutionary algorithms include crossover (or recombination), mutation, and selection. Evolutionary algorithms have been widely researched and applied in recent years due to their simple form, strong universality, and ability to obtain globally optimal solutions. Some improved evolutionary algorithms, such as memetic algorithms, after relying on global search capabilities to narrow the possible search range, combine efficient local optimal algorithms such as Tabu Search [29], Greedy Code Search (GCS) [30], etc., to optimize the search area to get the optimal solution.

2.2.1. Hybrid Evolutionary Algorithm Based on CAN

To leverage the advantages of global search and local search algorithms, this paper proposes a hybrid evolutionary algorithm called EA-CAN. By adopting evolutionary algorithms as the overarching framework, the algorithm exhibits strong global search capabilities, mitigating the risk of traditional gradient-based algorithms getting trapped in local optima. To address evolutionary algorithms' limited local refinement ability, the paper introduces the CAN algorithm, which offers efficient local optimization capabilities and computational efficiency as a local search algorithm [31]. As a result, the EA-CAN algorithm combines global search and local refinement capabilities.

Additionally, the time complexity of hybrid algorithms, such as the MA algorithm, is primarily determined by the time complexity of the local search algorithm. In this regard, introducing Fast Fourier Transform (FFT) significantly improves the time complexity of the local search compared to the general MA algorithm. Consequently, the overall computational efficiency of the algorithm is substantially enhanced.

Considering Q groups of phase-coded signals with a code length of P:

$$x_q(p) = c_{qp} = e^{j\varphi_q(p)}, \tag{5}$$

where $\varphi_q(p) \in [0, 2\pi)$, $p = 0, 1, \ldots, P-1$, $q = 0, 2, \ldots, Q-1$. Then the non-periodic cross-correlation function of the ith signal and the jth signal is defined as follows:

$$corr_{i,j}(k) = \sum_{p=0}^{P-1-k} x_i(p+k)x_j^*(p) = corr_{j,i}^*(-k) \tag{6}$$

where $i, j = 0, 2, \ldots, Q-1,\ k = 0, 1, \ldots, P-1$. When $i = j$, the above formula becomes the auto-correlation function of the ith signal. According to the actual working scenario of the radar, different orthogonal phase-coded signal optimization criteria can be selected [32]. This paper chooses the peak sidelobe as the cost function of the optimization algorithm, which can be expressed as:

$$E = \sum_{q=0}^{Q-1} \max\left|corr_{q,q}(k)\right| + \sum_{i=0}^{Q-1} \sum_{\substack{j=0 \\ j\neq i}}^{Q-1} \max\left|corr_{i,j}(k)\right|, \tag{7}$$

where $\max\left|corr_{q,q}(k)\right|$ is the peak sidelobe (Peak Sidelobe Level, PSL) of the qth signal, $\max\left|corr_{i,j}(k)\right|$ $(i, j = 0, 2, \ldots Q-1, i \neq j)$ is the peak cross-correlation level (Peak Cross-Correlation Level, PCCL) of the ith and jth signals. Usually, normalized PSL and PCCL are used as measurement indicators, divided by the auto-correlation peak and the code length N. The PSL and PCCL used in the following text refer to normalized values.

The EA-CAN algorithm process is shown in Algorithm 1, where the partial restart strategy is to randomly generate a specified number (partial restart individual number N_{st}) of new individuals at intervals of a specified number of generations (partial restart interval generation G_{rs}) during the evolution of the population and add them to the population to participate in the evolution of the population, to improve the diversity of the population. After each random generation of population individuals and random mutations, CAN will be used for local optimization. Then a new population will be formed or added to the original population. It should be noted that the local search algorithm CAN algorithm is optimized based on the integrated sidelobe level (Integrated Sidelobe Level, ISL), but this does not contradict the overall optimization criteria: choosing the peak sidelobe as the basis for selection ensures that the peak sidelobe continues to decline during the iteration process, while a local search is based on ISL as the criterion to avoid unrobust optimization results brought by only using the peak criterion.

Algorithm 1: EA-CAN Algorithm

Initialization:
Iteration times $i := 0$.
EA parameter initialization:
  Parent population individual number N_{par}, offspring population individual number N_{os}, partial restart individual number N_{rs}.
  Partial restart interval generation G_{rs}, maximum iteration times G_{max} and mutation bit number N_{mut}.
Randomly generate $N_{par} + N_{os}$ individuals as the initial population $\mathbf{P}(0)$, and use CAN for local optimization.
Take the top N_{par} individuals as parents according to the cost function.
Repeat:
  If the iteration times i is a multiple of G_{rs}, perform a partial restart:
    Randomly generate N_{rs} new individuals and add them to the parents $\mathbf{P}(i)_{par}$ after using CAN for local optimization.
  Generate offspring:
    Randomly select N_{os} times from the parents $\mathbf{P}(i)_{par}$.
    Perform N_{mut} bit random mutations respectively and get offspring $\mathbf{P}(i)_{os}$ after using CAN for local optimization.
  Take the N_{par} top individuals from the union of parents $\mathbf{P}(i)_{par}$ and offspring $\mathbf{P}(i)_{os}$ as the next generation parents $\mathbf{P}(i+1)_{par}$ according to the cost function.
  Iteration times $i := i + 1$.
Until the stop condition is met

2.2.2. Design Results

Two orthogonal phase-coded waveform sets were generated using the EA-CAN algorithm proposed in this paper, serving as the pulse modulation signal set for the PAPC-st-MIMO signal. The code length of waveform set 1 is $P = 64$, and the group number is $Q = 256$; the code length of waveform set 2 is $P = 400$, and the group number is $Q = 256$. The algorithm simulation parameters are set as follows: the number of individuals in the parent population is $N_{par} = 4N$, the number of individuals in the offspring population is $N_{os} = 20N$, the number of individuals in the partial restart is $N_{rs} = 10N$, the number of generations in the partial restart interval is $G_{rs} = 5$, the maximum number of iterations in the evolutionary algorithm is $G_{max} = 1000$, and the number of mutation bits is $N_{mut} = 2$. The performance of the waveform generated by the EA-CAN algorithm and the impact of the signal set parameters on the waveform performance are analyzed.

The average PSL and PCCL of the two signal sets designed using the EA-CAN algorithm are shown in Table 1. Figures 2 and 3 show the auto-correlation and cross-correlation results of the two signal sets designed using the EA-CAN algorithm, with different color lines representing different waveforms. It can be seen that the average PSL of the waveform with a code length of $P = 64$ reaches below -28 dB, the average PSL of the waveform with a code length of $P = 400$ reaches below -33 dB, and its average PCCL can approach -19 dB.

Table 1. The average PSL and PCCL of PAPC signal sets.

	***P* = 64**	***P* = 400**
PSL	−28.41 dB	−33.85 dB
PCCL	−12.31 dB	−18.79 dB

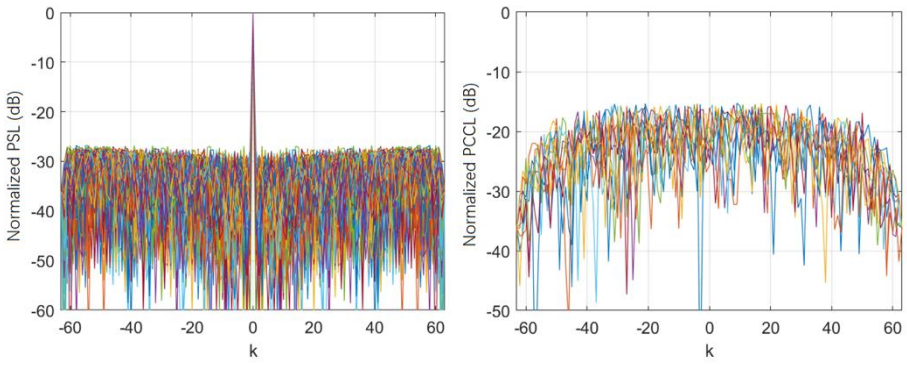

(**a**) (**b**)

Figure 2. Performance of PAPC signal set: $P = 64$, $Q = 256$. (**a**) Auto−correlation, (**b**) Cross−correlation.

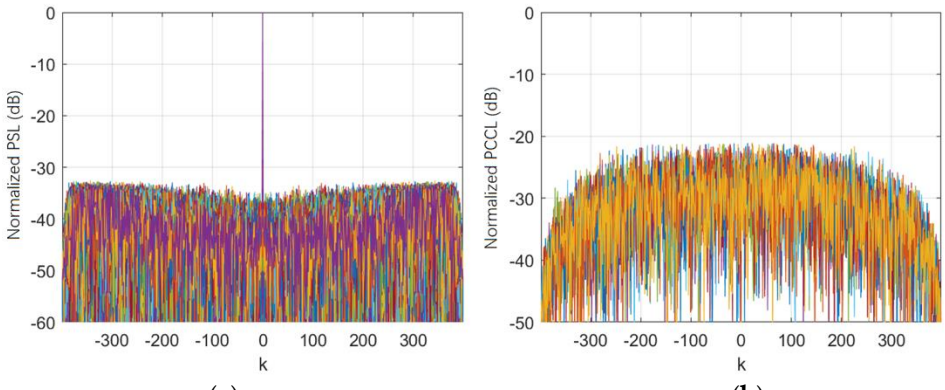

(**a**) (**b**)

Figure 3. Performance of PAPC signal set: $P = 400$, $Q = 256$. (**a**) Auto−correlation, (**b**) Cross−correlation.

The following gives the performance level of the EA-CAN algorithm when designing signal sets with different code lengths and numbers of signals. Figure 4a shows the changes in the average PSL and PCCL of the orthogonal phase-coded waveforms generated by the EA-CAN algorithm with the code length P, where $Q = 8$, P = 16, 32, 64, 128, 256, 512. To observe the trend of PSL and PCCL $1/\sqrt{N}$ is also plotted in the figure. Due to the increase in the code length P bringing more design degrees of freedom, both the average PSL and PCCL decrease with the increase in the code length P, and both fall at a velocity close to $O\left(1/\sqrt{N}\right)$.

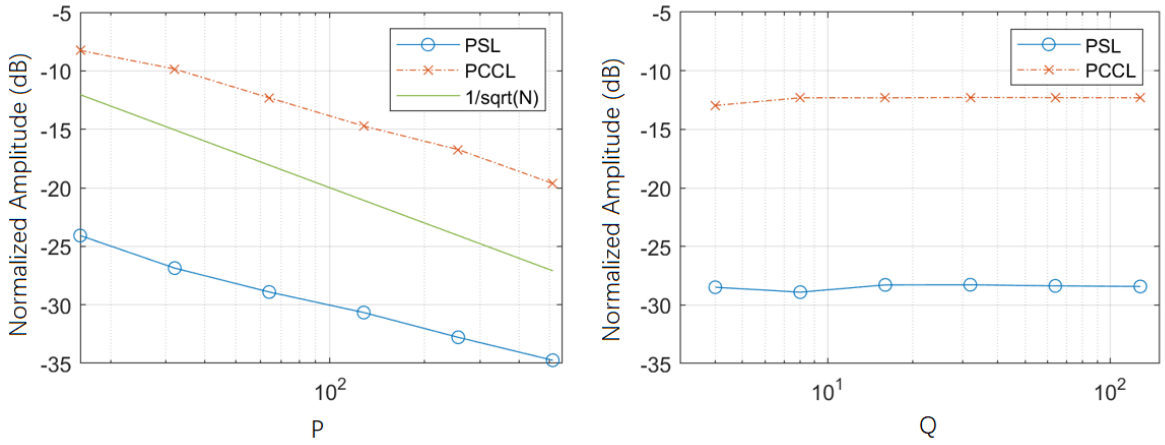

Figure 4. EA−CAN Algorithm Performance Analysis. (**a**) PSL and PCCL versus code length, (**b**) PSL and PCCL versus a number of signals.

Figure 4b shows the changes in the average PSL and PCCL of the orthogonal phase-coded waveforms generated by the EA-CAN algorithm with the number of signals Q, where $P = 64$, $Q = 4, 8, 16, 32, 64, 128$. The increase in the number of signals brings more constraints to the design, causing the average PSL and PCCL to increase with the increase in the number of signals Q. Overall, the choice of code length P has a more significant impact on the performance of the signal set designed by the EA-CAN algorithm.

2.3. PAPC-St-MIMO Signal Processing

The PAPC-st-MIMO waveform achieves range selectivity by utilising the PAPC signal set. In the signal processing procedure, the following steps are performed:

1. Different range segment filter groups are established and matched with the echo signal. The echo signal in other range segments is intentionally mismatched, resulting in the acquisition of one-dimensional range images for each range segment.
2. The echo pulse compression signal from different range segments undergoes processing using Pulse-Doppler (PD) techniques.
3. The traditional st-MIMO signal processing method is employed to demodulate the echo signal orthogonally. This step yields the echo signal for each MIMO receiving-transmitting channel at various ranges.
4. Finally, the imaging results from each range segment are merged or spliced together, enabling the retrieval of the echo signal for each MIMO receiving-transmitting channel after extending the detecting range.

Theoretically, the PAPC-st-MIMO waveform can obtain an unambiguous detecting range of $Q \times R_{prt}$, where $R_{prt} = 0.5cT_r$ is the unambiguous detecting range of a single pulse. The setting of the receiving filter group of different range segments of the PAPC-st-MIMO waveform and the range gating schematic is shown in Figure 5. The corresponding receiving filter group is set for different range segments, and the corresponding range segment echo can be coherently accumulated.

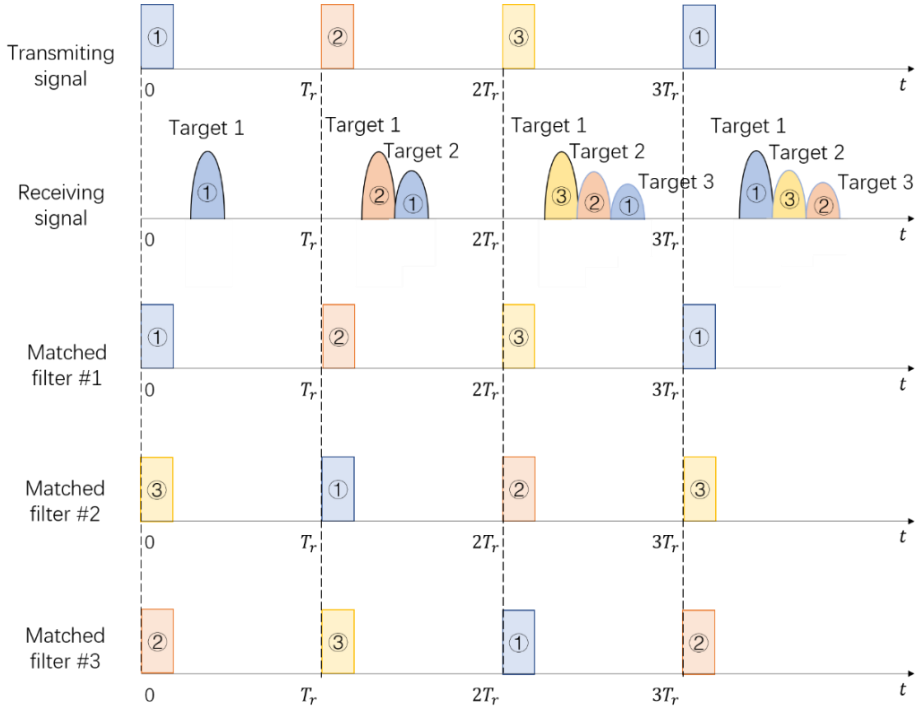

Figure 5. Diagram of range gating of PAPC-st-MIMO waveform.

The following establishes the echo model of the PAPC-st-MIMO signal under the unambiguous scenario and derives the processing process of the PAPC-DDMA signal. Based on the modeling process in Section 2.2.1, suppose a point target moving at a uniform velocity in the far field of the radar has a range of R_t from the radar, the radial velocity of the target relative to the radar is v_t, the corresponding target Doppler is $f_t = 2v_t/\lambda_0$, and the wave arrival direction of the target is ϕ_t. Then the echo signal received by the nth receiving antenna corresponding to the mth transmitting antenna can be expressed as:

$$s_{mn}(t) = \sum_{r=0}^{K/Q-1} \sum_{q=0}^{Q-1} u_{pulse}^{q}\left(t - \tau_{mn} - qT_r - rT_Q\right) e^{j2\pi f_0 (t-\tau_{mn})} e^{j2\pi(\alpha_m + f_t)(r\times Q+q)T_r}, \quad (8)$$

where τ_{mn} is the echo delay, which has the following form:

$$\tau_{mn} = \frac{2\left[R_t - v_t\left(qT_r + rT_Q\right)\right]}{c} - \frac{d_m \sin\phi_t}{c} - \frac{d_n \sin\phi_t}{c}. \quad (9)$$

Further, the received signal of the nth receiving antenna should be the sum of all M transmitted signals. After down-conversion and low-pass filtering, it can be expressed as:

$$X_n(t) = \sum_{m=0}^{M-1} \sum_{r=0}^{K/Q-1} \sum_{q=0}^{Q-1} u_{pulse}^{q}\left(t - \tau_{mn} - qT_r - rT_Q\right) e^{j2\pi f_0 \tau_{mn}} e^{j2\pi(\alpha_m + f_t)(r\times Q+q)T_r}. \quad (10)$$

Then, the echo signals received by each receiving antenna are jointly pulse-Doppler processed in multiple range segments to obtain a comprehensive range-Doppler plane without range ambiguity in multiple range segments. Use different receiving filter groups to match filter processing the received signal and obtain the matched filter output results corresponding to different range segments. Theoretically, a frame with Q groups of different codewords of the PAPC signal set can achieve up to Q unambiguous detection of range segments. As shown in Figure 5, the receiving filter group corresponding to the qth range segment should be obtained by cyclically shifting the baseband reference signal $u_{ref}(t)$ of the PAPC signal set by q pulses. Then the matched filter output result corresponding to the qth range segment can be expressed as:

$$\begin{aligned} s_{pc}^{q}(t) &= X_n(t) * h_q(t) \\ &= \int_{-\infty}^{\infty} X_n(\tau) h_q^*(t-\tau) d\tau, \end{aligned} \tag{11}$$

where $h_q(t)$ is the matched filter.

Rearrange the matched filter output result of the qth range segment according to the pulse repetition interval, perform slow-time pulse-Doppler processing, that is, perform windowing, zero-padding, and discrete Fourier transform along the slow time, and obtain the range-Doppler plane corresponding to each range segment. Splice the range-Doppler planes corresponding to each segment in sequence to obtain a comprehensive range-Doppler plane of multiple range segments. The result of the FFT processing of the matched filter output result $s_{pc}^{q}(t)$ of the qth range segment rearranged according to the number of pulses has the following form:

$$y_{pd}^{q}(t,l) = \sum_{k=0}^{K-1} w(k) x_n^k(t) e^{-j2\pi k \frac{l}{L}}, \tag{12}$$

where $w(k)$ is the weight value of the slow-time window function, used to suppress the sidelobe of the velocity dimension, and $x_n^k(t)$ is the kth pulse of the matched filter output result of the qth range segment, and $l = 0, \cdots, L-1$ represents the output of the lth velocity channel. Splice the pulse-Doppler processing results corresponding to each range segment in sequence to obtain a comprehensive range-Doppler plane of multiple range segments that is:

$$y_{pd\_All}^{n}(t,l) = \sum_{q=0}^{Q-1} y_{pd}^{q}(t - qT_r, l). \tag{13}$$

Finally, use the Doppler filter to demodulate the comprehensive range-Doppler plane corresponding to each receiving antenna of the MIMO and obtain the comprehensive range-Doppler plane after demodulation of each MIMO receiving-transmitting channel. To separate the response of the ith transmitting antenna on the comprehensive range-Doppler plane corresponding to the nth receiving antenna, use the Doppler frequency center α_i corresponding to the ith transmitting channel to mix with $y_{pd\_All}^{n}(t,l)$ to get the echo corresponding to the ith transmitting channel with zero Doppler:

$$\widetilde{y}_{pd\_All}^{n,i}(t,l) = y_{pd\_All}^{n}(t,l) \cdot e^{-j2\pi\alpha_i k T_r}. \tag{14}$$

Then, use a low-pass filter with a cutoff frequency of $[-\Delta f_{sub}/2, \Delta f_{sub}/2]$ to process $\widetilde{y}_{pd\_All}^{n,i}(t,l)$, and obtain the comprehensive range-Doppler plane corresponding to the (n,i)th receiving-transmitting channel:

$$y_{pd\_All}^{n,i}(t,l) = \widetilde{y}_{pd\_All}^{n,i}(t,l) * H_{LP}(t,l), \tag{15}$$

where $H_{LP}(t,l)$ is the time-domain response of the low-pass filter. This way, the comprehensive range-Doppler plane corresponding to each MIMO receiving-transmitting channel can be obtained, and slow-time MIMO demodulation can be realized.

The complete PAPC-st-MIMO signal processing process is shown in Algorithm 2:

Algorithm 2: PAPC-st-MIMO Signal Processing

Begin:
Target parameter initialization.
Received PAPC-DDMA signals of each channel.
Initial range segment $q = 0$.
While $q \neq Q$**:**
  Select q.
  Matched filtering using the receive filter for the current range segment.
  Pulse-Doppler processing for the current range segment.
  Select next $q + 1$.
End
Synthetic Range-Doppler plot for multiple range segments.
MIMO demodulation using Doppler filters.
Synthetic Range-Doppler plot for multiple range segments of each receiver-transmitter channel.
CFAR detection.
End

3. Simulation and Analysis

This section validates the range selectivity performance of the PAPC-st-MIMO waveform through simulation experiments. The experimental setup considers a one-dimensional MIMO antenna array arranged along the pitch direction with co-located transceivers. The array consists of 6 elements, where each antenna transmits the PAPC-st-MIMO waveform.

For the PAPC signal set, signals 1 and 2, described in Section 2.2.2, are utilized. These signal sets correspond to near and far radar detection scenarios, respectively. Targets are placed at different range segments, and their performance is compared with that of the slow-time MIMO (LFM-st-MIMO) waveforms, where the intra-pulse modulation involves Linear Frequency Modulation signals. By conducting these experiments, the proposed range ambiguity suppression method based on PAPC-st-MIMO is validated.

3.1. Near-Range Detection Scenario

This simulation uses a PAPC signal set 1 with a code length $P = 64$ and group number $Q = 256$ as the intra-pulse modulated PCPA-st-MIMO waveform. Specific waveform parameters and detection performance are shown in Tables 2 and 3. The radar's instantaneous bandwidth is 40 MHz, corresponding to a chip width of 0.025 µs. When using a PAPC signal set 1 with a code length, the corresponding pulse width is 1.6 µs. The radar pulse repetition interval is set to 10 µs, corresponding to a radar unambiguous range measurement of 1.5 km. The PAPC signal set with group number can theoretically achieve unambiguous joint detection of 256 range segments. To simplify the process, the number of combined range segments is set to 4, i.e., the combined unambiguous range after multi-range segment combined processing is 6 km. The number of transmit channels is set to 6, and the number of Doppler sub-bands is 8, including two redundant Doppler sub-bands. The number of coherently processed pulses within one CPI is 1024, i.e., the coherent processing period is 10.24 ms, corresponding to the unambiguous velocity measurement range of $\pm$302.4 m/s.

Four simulation targets with different ranges, velocities, and signal-to-noise ratios (SNRs) were set, as shown in Table 4. Each target was located in a different range segment, and the post-compression SNR for each target was set to 20 dB. For traditional slow-time MIMO waveforms based on LFM, targets 2, 3, and 4 would generate range ambiguities.

After matched filtering and pulse-Doppler processing, the multi-range joint Range-Doppler (RD) plane of the PAPC-st-MIMO waveform is shown in Figure 6a. The single-channel multi-range joint RD plane after slow-time MIMO demodulation is shown in Figure 6b. The processing results of the traditional LFM-st-MIMO waveform are shown in Figure 7. For ease of comparison, the processing results of the LFM-st-MIMO waveform for the four range ranges are also listed. The PAPC-st-MIMO waveform has range selectivity, and it can effectively suppress ambiguous echoes generated by each target at other corre-

sponding range ranges, achieving unambiguous multi-range joint detection results. This allows the radar system to maintain its original unambiguous velocity measurement range without decreasing the pulse repetition frequency to achieve a greater unambiguous range scope. In contrast, traditional LFM-st-MIMO waveforms generate ambiguous echoes at other corresponding range ranges, which could lead to false alarms and inaccurate target range information.

Table 2. Short Pulse Waveform Parameters.

Variable	Value
Initial Carrier Frequency	3.1 GHz
Instantaneous Bandwidth	40 MHz
Pulse Width	1.6 μs
Sampling Frequency	80 MHz
Pulse Repetition Interval	10 μs
Chip Width	0.025 μs
Number of Code Elements	64
Number of Accumulated Pulses within CPI	1024
Number of Pulses within Frame	256
Number of Transmit Channels	6
Number of Doppler Sub-bands	8
Number of Combined Range Segments	4

Table 3. Short Pulse Waveform Detection Performance.

Variable	Value
Range Resolution	3.75 m
Velocity Resolution	4.7 m/s
Unambiguous Velocity Range of Doppler Sub-band	±302.4 m/s
Unambiguous Range of Single Pulse	1.5 km
Combined Unambiguous Range	6 km

Table 4. Parameters for Targets in a Near-Range Scenario Parameter.

Parameter	Target 1	Target 2	Target 3	Target 4
Target Range	0.5 km	2.1 km	3.7 km	5.3 km
Target Velocity	60 m/s	20 m/s	−20 m/s	−60 m/s
SNR	20 dB	20 dB	20 dB	20 dB
Located Range Segment	1	2	3	4

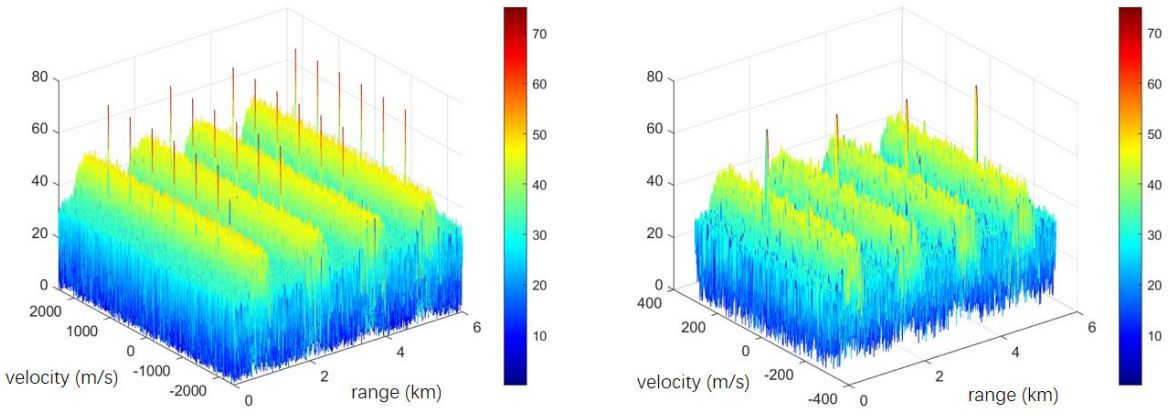

(**a**) (**b**)

Figure 6. Near−range scenario PAPC−st−MIMO range−velocity plane. (**a**) Range−velocity plane before demodulation, (**b**) Range−velocity plane after demodulation.

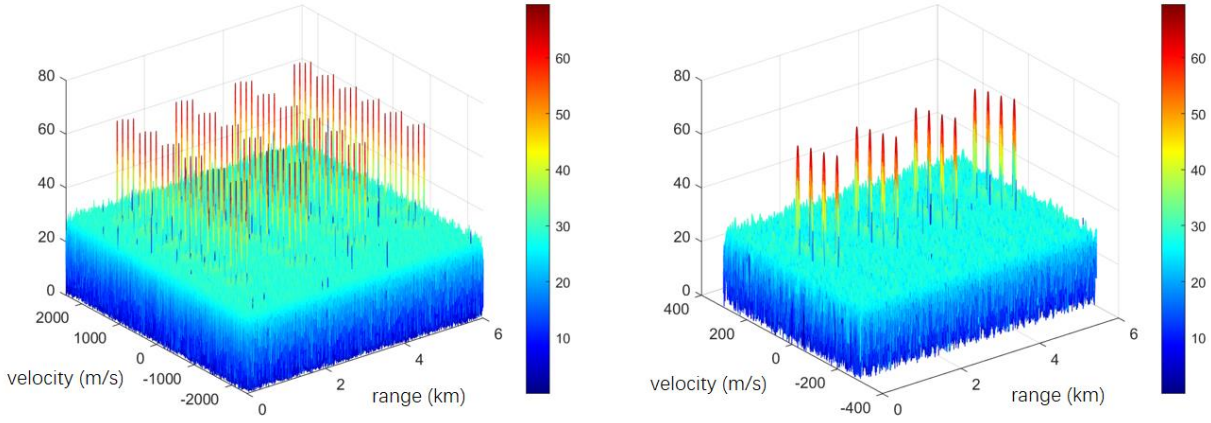

(**a**) (**b**)

Figure 7. Near−range scenario LFM−st−MIMO range−velocity plane. (**a**) Range−velocity plane before demodulation, (**b**) Range−velocity plane after demodulation.

Figures 8 and 9 further display the one-dimensional range image of the PAPC-st-MIMO and LFM-st-MIMO signals for each target in the velocity channel, with the range and amplitude information of each target echo, noted. The PAPC-st-MIMO signal can achieve unambiguous multi-range joint detection of targets and obtain accurate target range information. After PD processing, the theoretical target SNR is 50 dB. The average target SNR obtained after processing the PAPC-st-MIMO waveform is 49.8 dB, consistent with the theoretical value. In contrast, LFM-st-MIMO signal targets will generate ambiguous targets at intervals of the single pulse unambiguous ranging scope of 1.5 km. Due to the two-dimensional window processing of range and velocity, the average target SNR obtained after processing the LFM-DDMA waveform is 47.4 dB, a loss of 2.6 dB compared to the theoretical value. Figure 10 shows the velocity spectra of the PAPC-st-MIMO signals for targets in different range units. By slow-time MIMO demodulation of the combined range-Doppler plane over multiple range segments, accurate target velocity information can be obtained.

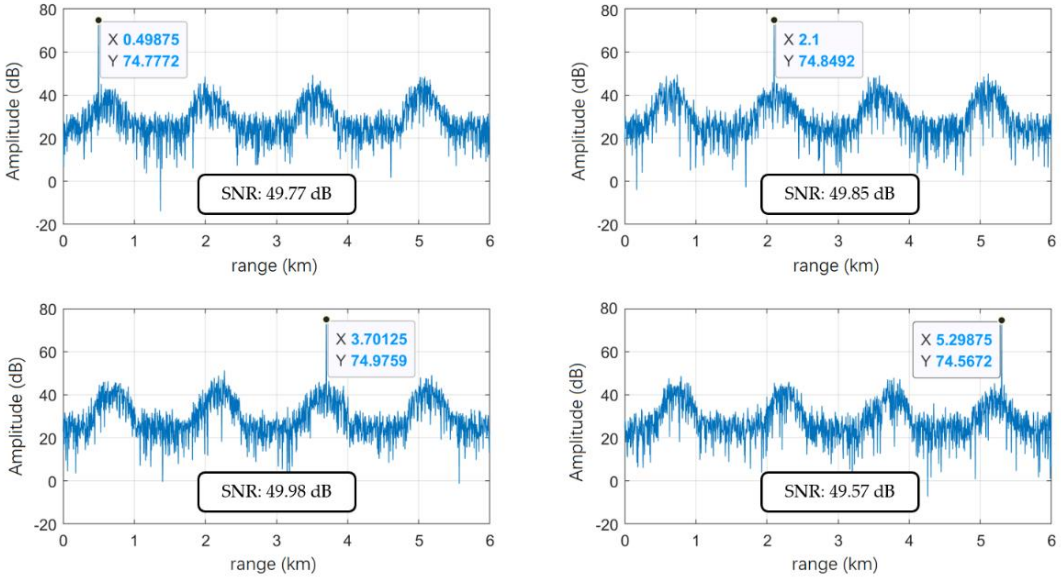

Figure 8. Near−range scenario PAPC−st−MIMO one−dimensional range image of each target in the velocity channel, with SNRs are 49.77, 49.85, 49.98 and 49.57 dB, respectively.

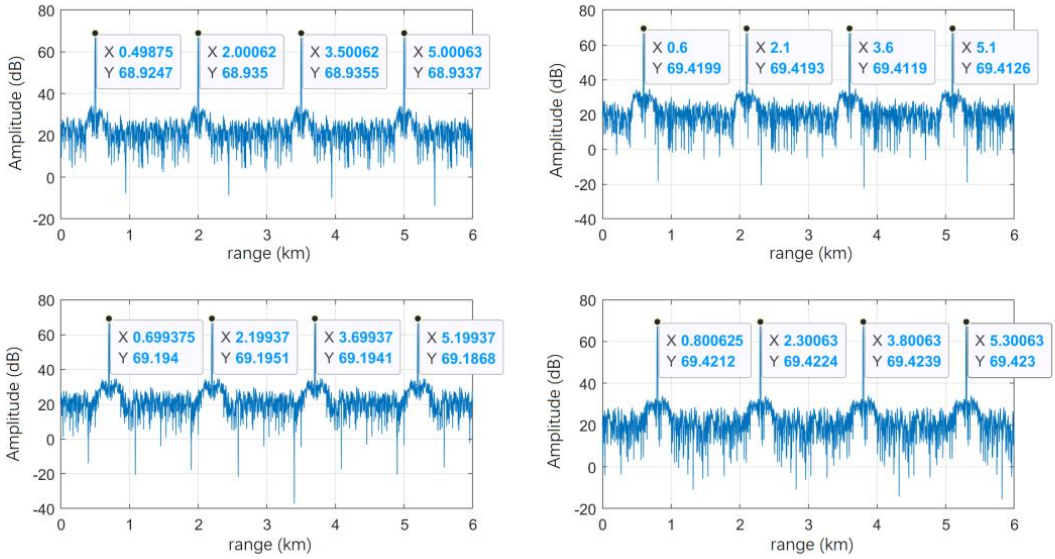

Figure 9. Near−range scenario LFM−st−MIMO one−dimensional range image of each target in the velocity channel.

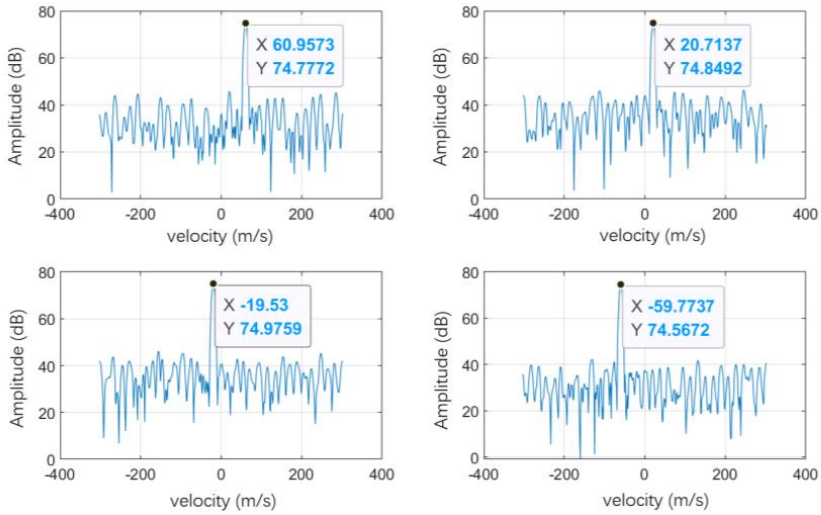

Figure 10. Velocity spectra of the PAPC−st−MIMO signal for targets in different range units in a near-range scenario.

As can also be seen from Figure 8, although the PAPC-st-MIMO signal has range selectivity, targets in each range segment can form higher sidelobes in other range segments, and the level of these sidelobes is constrained by the cross-correlation level of the PAPC signal set. Under the parameters of this group of simulations, the sidelobe level of the range segment for the PAPC-st-MIMO signal corresponding to the PAPC coding set, with a code length $P = 64$ and group number $Q = 256$, is -30.1 dB.

3.2. Long-Range Detection Scenario

This subsection presents a simulation experiment using a PAPC signal set 2, with a code length $P = 400$ and a group number $Q = 256$, as the intra-pulse modulated PCPA-st-MIMO waveform. The specific waveform parameters and detection performance are shown in Tables 5 and 6. The radar instantaneous bandwidth is set to 40 MHz. When the PAPC signal set 2 with the code length $P = 400$ is used, the corresponding pulse width is 10 μs. The radar pulse repetition interval is set to 40 μs, corresponding to a radar unambiguous range measurement of 6 km. The number of combined range segments is set to 4, meaning the combined unambiguous range measurement after multi-range segment

composite processing is 24 km. The number of coherently processed pulses within a CPI is 1024, i.e., the coherent processing period is 40.96 ms, corresponding to an unambiguous velocity measurement range of ±75.6 m/s in the Doppler sub-band.

Table 5. Long Pulse Waveform Parameters.

Variable	Value
Initial Carrier Frequency	3.1 GHz
Instantaneous Bandwidth	40 MHz
Pulse Width	10 μs
Sampling Frequency	80 MHz
Pulse Repetition Interval	40 μs
Chip Width	0.025 μs
Number of Chips	400
Accumulated Pulses within CPI	1024
Pulses per Frame	256
Number of Transmit Channels	6
Number of Doppler Sub-bands	8
Number of Combined Range Segments	4

Table 6. Long Pulse Waveform Detection Performance.

Variable	Value
Range Resolution	3.75 m
Velocity Resolution	1.2 m/s
Unambiguous Velocity Measurement Range in Doppler Sub-band	±75.6 m/s
Unambiguous Range Measurement per Pulse	6 km
Combined Unambiguous Range Measurement	24 km

Four simulation targets with different ranges, velocities, and signal-to-noise ratios are set up, as shown in Table 7, each located in four range segments. The signal-to-noise ratio for each target after pulse compression is set to 20 dB. For traditional slow-time MIMO waveforms based on LFM, targets 2, 3, and 4 would all produce range ambiguities.

Table 7. Parameters of Targets in a Long-Range Scenario Parameter.

Parameter	Target 1	Target 2	Target 3	Target 4
Target Range	3 km	9.1 km	15.2 km	21.3 km
Target Velocity	40 m/s	10 m/s	−10 m/s	−40 m/s
SNR	20 dB	20 dB	20 dB	20 dB
Located Range Segment	1	2	3	4

The combined Range-Doppler (RD) plane for multiple range segments of PAPC-st-MIMO waveform after matched filtering and pulse-Doppler processing is shown in Figure 11a. The single-channel combined RD plane for multiple range segments after slow-time MIMO demodulation is shown in Figure 11b, while the result using traditional LFM-st-MIMO waveform is shown in Figure 12. As can be observed, the PAPC-st-MIMO waveform features range-selective properties. It effectively suppresses ambiguous echoes produced by each target at corresponding positions in other range segments, leading to unambiguous combined detection results for multiple range segments. Conversely, the traditional LFM-st-MIMO waveform generates ambiguous echoes at corresponding positions in other range segments, causing false alarms and failing to yield accurate target range information.

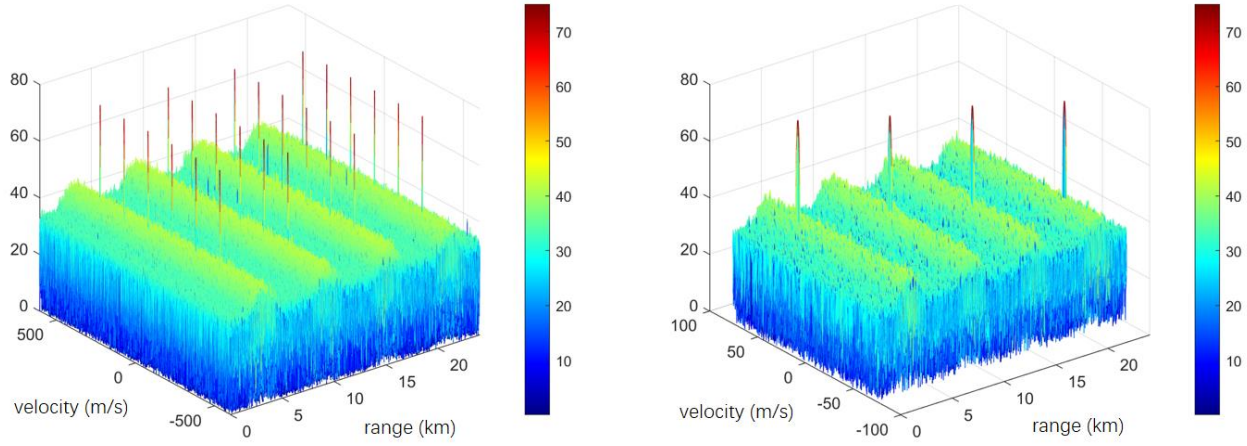

(**a**) (**b**)

Figure 11. Range−velocity plane of PAPC−st−MIMO in a long−range scenario. (**a**) Range−velocity plane before demodulation, (**b**) Range−velocity plane after demodulation.

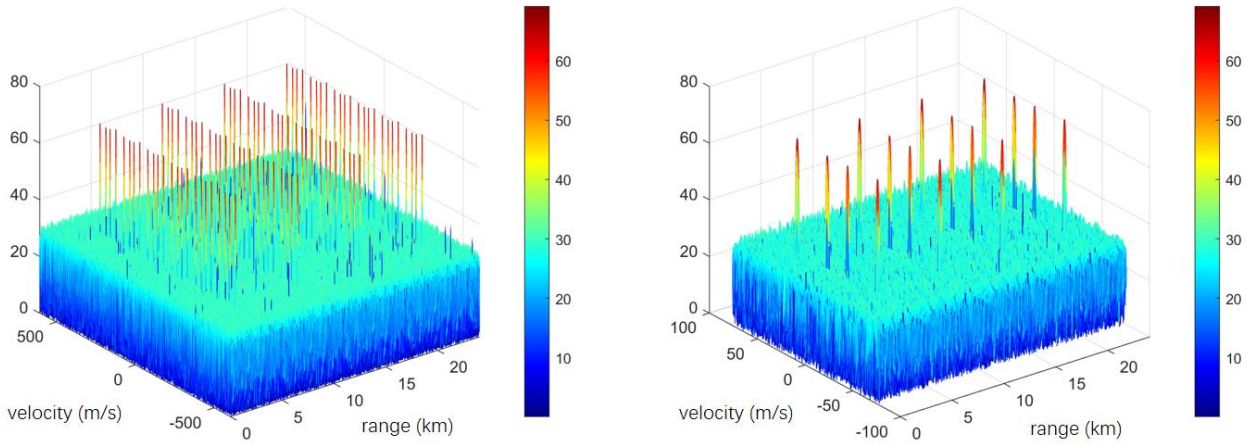

(**a**) (**b**)

Figure 12. Range−velocity plane of LFM−st−MIMO in a long−range scenario. (**a**) Range−velocity plane before demodulation, (**b**) Range−velocity plane after demodulation.

Figures 13 and 14 further present one-dimensional range images of the velocity channels where each target resides for PAPC-st-MIMO and LFM-st-MIMO signals, with each target's echo range and amplitude information noted. It can be seen that the PAPC-st-MIMO signal can achieve unambiguous joint detection of targets over multiple range segments, providing accurate target range information. After PD processing, the average signal-to-noise ratio of the targets obtained after processing the PAPC-st-MIMO waveform is 49.8 dB, consistent with the theoretical value. Under the parameters of this simulation, the sidelobe level of the range segment of the PAPC-st-MIMO signal corresponding to the PAPC coding set with a code length $P = 400$ and a group number $Q = 256$ is -35.1 dB. LFM-st-MIMO signals will generate ambiguous targets at intervals of the unambiguous range measurement of 6 km per pulse. Influenced by the two-dimensional window processing of range and velocity, the average signal-to-noise ratio of the targets is 47.5 dB, a loss of 2.5 dB compared to the theoretical value. Figure 15 shows the velocity spectra of the range units where each target of the PAPC-st-MIMO signal resides. It can be seen that by conducting slow-time MIMO demodulation on the combined range-Doppler plane of multiple range segments, accurate target velocity information can be obtained.

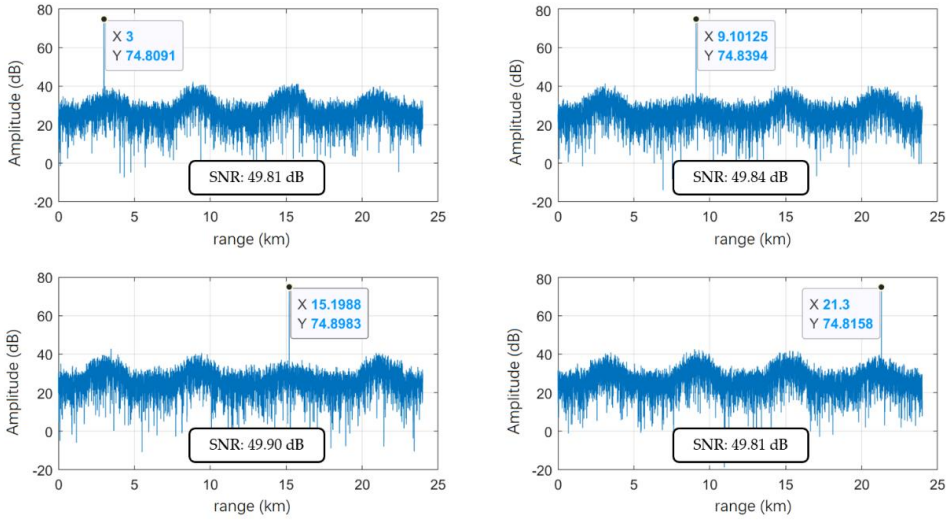

Figure 13. One−dimensional range image of each target's velocity channel of PAPC−st−MIMO in a long−range scenario, with SNRs are 49.81, 49.84, 49.90 and 49.81 dB, respectively.

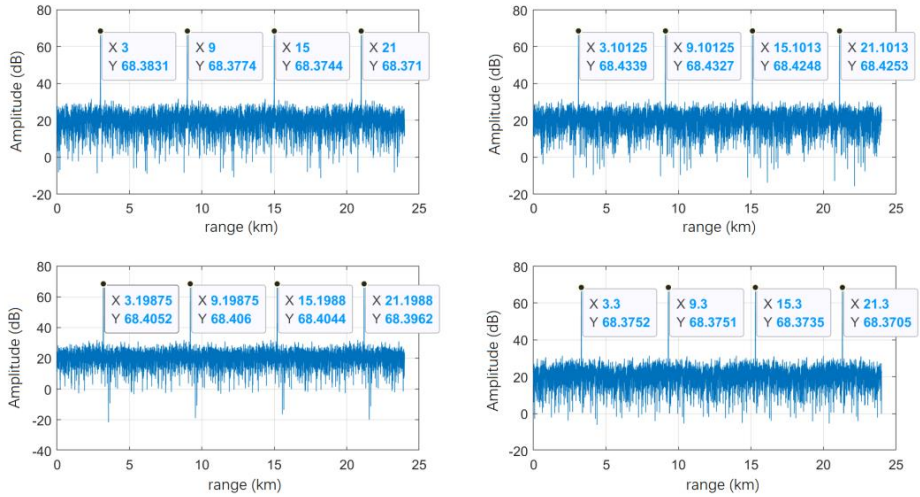

Figure 14. One−dimensional range image of each target's velocity channel of LFM−st−MIMO in a long−range scenario.

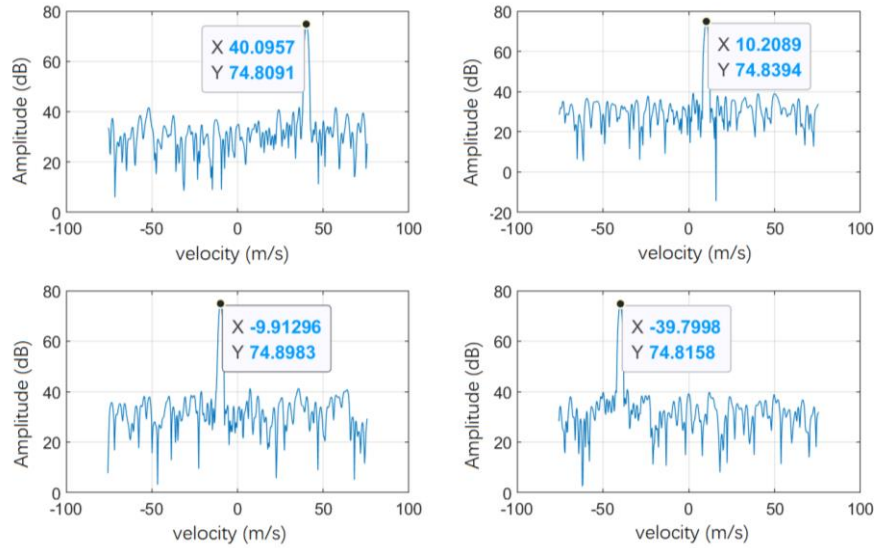

Figure 15. Velocity spectra of each target's range unit of PAPC−st−MIMO in a long-range scenario.

4. Conclusions

This paper proposed a Pulse-Agile-Phase-Coding slow-time MIMO (PAPC-st-MIMO) waveform, where the phase-coded signal is utilized as the intra-pulse modulation of the slow-time MIMO waveform. To improve the orthogonality of the phase-coded waveform sets, a novel hybrid evolutionary algorithm based on CAN is proposed. After the optimization process of the phase-coded waveform sets, the signal processing method of the PAPC-st-MIMO waveform is derived. This approach ensures waveform orthogonality while enabling the slow-time MIMO waveform to achieve distance selectivity. By conducting joint pulse-Doppler processing across multiple range segments, range ambiguity can be suppressed, increasing the system's PRF without introducing ambiguity. The effectiveness of the proposed method is verified with a simulation experiment. The advantages of the proposed method are mainly reflected in lower sidelobe, more concise structure, and lower computational complexity.

Author Contributions: Conceptualization, S.C. and F.Y.; methodology, S.C.; software, F.Y.; validation, S.C. and F.Y.; formal analysis, S.C. and Z.L.; investigation, S.C. and F.Y.; writing—original draft preparation, S.C.; writing—review and editing, F.Y., W.R. and Z.L.; visualization, F.Y. and H.Z.; supervision, Q.L.; project administration, Z.L.; funding acquisition, Q.L. All authors have read and agreed to the published version of the manuscript.

Funding: This research was partly funded by the Beijing Institute of Technology Research Fund Program for Young Scholars under Grant XSQD202205012 and partly by the National Natural Science Foundation of China, under Grant 62201048.

Data Availability Statement: The data that support the findings of this study are available from the corresponding author, Z.L., upon reasonable request.

Acknowledgments: The authors thank the editor and anonymous reviewers for their helpful comments and suggestions.

Conflicts of Interest: The authors declare no conflict of interest.

References

1. Fishler, E.; Haimovich, A.; Blum, R.; Chizhik, D.; Cimini, L.; Valenzuela, R. MIMO radar: An idea whose time has come. In Proceedings of the 2004 IEEE Radar Conference (IEEE Cat. No. 04CH37509), Philadelphia, PA, USA, 26–29 April 2004; IEEE: Piscataway, NJ, USA, 2004; pp. 71–78.
2. Bliss, D.; Forsythe, K.W.; Davis, S.K.; Fawcett, G.S.; Rabideau, D.J.; Horowitz, L.L.; Kraut, S. Gmti mimo radar. In Proceedings of the 2009 International Waveform Diversity and Design Conference, Kissimmee, FL, USA, 8–13 February 2009; IEEE: Piscataway, NJ, USA, 2009; pp. 118–122.
3. Forsythe, K.; Bliss, D.; Fawcett, G. Multiple-input multiple-output (MIMO) radar: Performance issues. In Proceedings of the Conference Record of the Thirty-Eighth Asilomar Conference on Signals, Systems and Computers, Pacific Grove, CA, USA, 7–10 November 2004; IEEE: Piscataway, NJ, USA, 2004; Volume 1, pp. 310–315.
4. Fishler, E.; Haimovich, A.; Blum, R.; Cimini, R.; Chizhik, D.; Valenzuela, R. Performance of MIMO radar systems: Advantages of angular diversity. In Proceedings of the Conference Record of the Thirty-Eighth Asilomar Conference on Signals, Systems and Computers, Pacific Grove, CA, USA, 7–10 November 2004; IEEE: Piscataway, NJ, USA, 2004; Volume 1, pp. 305–309.
5. Li, J.; Stoica, P. *MIMO Radar Signal Processing*; John Wiley & Sons: Hoboken, NJ, USA, 2008.
6. Lan, L.; Marino, A.; Aubry, A.; De Maio, A.; Liao, G.; Xu, J.; Zhang, Y. GLRT-based Adaptive Target Detection in FDA-MIMO Radar. *IEEE Trans. Aerosp. Electron. Syst.* **2020**, *57*, 597–613. [CrossRef]
7. Mecca, V.F.; Krolik, J.L.; Robey, F.C. Beamspace slow-time MIMO radar for multipath clutter mitigation. In Proceedings of the 2008 IEEE International Conference on Acoustics, Speech and Signal Processing, Las Vegas, NV, USA, 31 March–4 April 2008; IEEE: Piscataway, NJ, USA, 2008; pp. 2313–2316.
8. Krolik, J.; Mecca, V.; Kazanci, O.; Bilik, I. Multipath spread-Doppler clutter mitigation for over-the-horizon radar. In Proceedings of the 2008 IEEE Radar Conference, Rome, Italy, 26–30 May 2008; IEEE: Piscataway, NJ, USA, 2008; pp. 1–5.
9. Bilik, I.; Kazanci, O.; Krolik, J. Radar clutter mitigation via space-time wavefront adaptive sensing. In Proceedings of the 2008 IEEE International Conference on Acoustics, Speech and Signal Processing, Las Vegas, NV, USA, 31 March–4 April 2008; IEEE: Piscataway, NJ, USA, 2008; pp. 2589–2592.
10. Lan, L.; Xu, J.; Liao, J.; Zhang, Y.; Fioranelli, F.; So, H.C. Suppression of mainbeam deceptive jammer with FDA-MIMO radar. *IEEE Trans. Veh. Technol.* **2020**, *69*, 11584–11598. [CrossRef]

11. Zhao, Z.; Chen, J.; Bao, Z. Slow time random phase-coded waveforms in MIMO OTHR. In Proceedings of the ISAPE2012, Xi'an, China, 22–26 October 2012; IEEE: Piscataway, NJ, USA, 2012; pp. 1195–1198.
12. Mecca, V.F.; Krolik, J.L.; Robey, F.C.; Ramakrishnan, D.; Li, J.; Stoica, P. Slow-time MIMO spacetime adaptive processing. In *MIMO Radar Signal Processing*; John Wiley & Sons: Hoboken, NJ, USA, 2009; pp. 283–318.
13. Kantor, J.M.; Bliss, D.W. Clutter covariance matrices for GMTI MIMO radar. In Proceedings of the 2010 Conference Record of the Forty Fourth Asilomar Conference on Signals, Systems and Computers, Pacific Grove, CA, USA, 7–10 November 2010; IEEE: Piscataway, NJ, USA, 2010; pp. 1821–1826.
14. Kantor, J.; Davis, S.K. Airborne GMTI using MIMO techniques. In Proceedings of the 2010 IEEE Radar Conference, Arlington, VA, USA, 10–14 May 2010; IEEE: Piscataway, NJ, USA, 2010; pp. 1344–1349.
15. Forsythe, K.W.; Bliss, D.W. MIMO radar waveform constraints for GMTI. *IEEE J. Sel. Top. Signal Process.* **2010**, *4*, 21–32. [CrossRef]
16. Xu, F.; Vorobyov, S.A.; Yang, F. Transmit beamspace DDMA based automotive MIMO radar. *IEEE Trans. Veh. Technol.* **2021**, *71*, 1669–1684. [CrossRef]
17. Yang, F.; Le Kernec, J.; Fioranelli, F.; Liu, Q. Shape feature aided target detection method for micro-drone surveillance radar. In Proceedings of the IET International Radar Conference (IET IRC 2020), Online, 4–6 November 2020.
18. Yang, F.; Qu, K.; Hao, M.; Liu, Q.; Chen, X.; Xu, F. Practical investigation of a MIMO radar system for small drones detection. In Proceedings of the 2019 International Radar Conference (RADAR), Toulon, France, 23–27 September 2019; IEEE: Piscataway, NJ, USA, 2019; pp. 1–5.
19. AWR1843 Data Sheet, Product Information and Support by Texas Instruments. Available online: https://www.ti.com/product/AWR1843/ (accessed on 1 April 2023).
20. Malik, H.; Burki, J.; Ali, M.S.; Salman, A. Experimental Results for Angular Resolution Improvement in Slow-Time Phase-Coded FMCW MIMO Radars. In Proceedings of the 2021 International Bhurban Conference on Applied Sciences and Technologies (IBCAST), Islamabad, Pakistan, 12–16 January 2021; IEEE: Piscataway, NJ, USA, 2021; pp. 1011–1016.
21. Yang, F.; Guo, J.; Zhu, R.; Le Kernec, J.; Liu, Q.; Zeng, T. Ground Clutter Mitigation for Slow-Time MIMO Radar Using Independent Component Analysis. *Remote Sens.* **2022**, *14*, 6098. [CrossRef]
22. Yang, F.; Xu, F.; Fioranelli, F.; Le Kernec, J.; Chang, S.; Long, T. Practical investigation of a MIMO radar system capabilities for small drones detection. *IET Radar Sonar Navig.* **2021**, *15*, 760–774. [CrossRef]
23. Rabideau, D.J. Doppler-offset waveforms for MIMO radar. In Proceedings of the 2011 IEEE RadarCon (RADAR), Kansas City, MO, USA, 23–27 May 2011; IEEE: Piscataway, NJ, USA, 2011; pp. 965–970.
24. Rabideau, D.J. MIMO radar waveforms and cancellation ratio. *IEEE Trans. Aerosp. Electron. Syst.* **2012**, *48*, 1167–1178. [CrossRef]
25. van Rossum, W.; Anitori, L. Doppler ambiguity resolution using random slow-time code division multiple access MIMO radar with sparse signal processing. In Proceedings of the 2018 IEEE Radar Conference (RadarConf18), Oklahoma City, OK, USA, 23–27 April 2018; IEEE: Piscataway, NJ, USA, 2018; pp. 0441–0446.
26. Li, F.; He, F.; Dong, Z.; Wu, M.; Zhang, Y.; Sun, Z. Blind velocities mitigation for DDMA MIMO GMTI radar via multi-frequency signals. In Proceedings of the 2018 19th International Radar Symposium (IRS), Bonn, Germany, 20–22 June 2018; IEEE: Piscataway, NJ, USA, 2018; pp. 1–9.
27. Wang, L.; Li, B.; Yu, C.; Liu, A.; Ji, X. PARAFAC-Direct: A Joint Parameters Estimation Method for Slow-Time MIMO. *IEEE Signal Process. Lett.* **2022**, *29*, 732–736. [CrossRef]
28. Mow, W.H.; Du, K.L.; Wu, W.H. New evolutionary search for long low autocorrelation binary sequences. *IEEE Trans. Aerosp. Electron. Syst.* **2015**, *51*, 290–303. [CrossRef]
29. Liu, D.; Liu, Y.; Cai, H. Orthogonal polyphase code sets design for MIMO radar using tabu search. In Proceedings of the 2012 IEEE International Conference on Intelligent Control, Automatic Detection and High-End Equipment, Beijing, China, 27–29 July 2012; IEEE: Piscataway, NJ, USA, 2012; pp. 123–127.
30. Ren, W.; Zhang, H.; Liu, Q.; Yang, Y. Greedy code search based memetic algorithm for the design of orthogonal polyphase code sets. *IEEE Access* **2019**, *7*, 13561–13576. [CrossRef]
31. Stoica, P.; He, H.; Li, J. New algorithms for designing unimodular sequences with good correlation properties. *IEEE Trans. Signal Process.* **2009**, *57*, 1415–1425. [CrossRef]
32. Nunn, C. Constrained optimization applied to pulse compression codes and filters. In Proceedings of the IEEE International Radar Conference, Arlington, VA, USA, 9–12 May 2005; IEEE: Piscataway, NJ, USA, 2005; pp. 190–194.